Electrodeposited Nickel-Zinc Alloy Nanostructured Electrodes for Alkaline Electrolyzer

F. Ganci[1], B. Buccheri[1], B. Patella[1], E. Cannata[1], G. Aiello[1], P. Mandin[2], R. Inguanta[1]

[1]Dipartimento di Ingegneria, Università di Palermo, Viale delle Scienze, 90128 Palermo, Italy

[2]Université Bretagne Sud, IRDL UMR CNRS 6027, 56100 Lorient, France

Corresponding author: rosalinda.inguanta@unipa.it

ABSTRACT

Over the last decade, as a consequence of the global decarbonization process, the interest towards green hydrogen production has drastically increased. In particular a substantial research effort has focused on the efficient and affordable production of carbon-free hydrogen production processes. In this context, the development of more efficient electrolyzers with low-cost electrode/electrocatalyst materials can play a key role. This work, investigates the fabrication of electrodes of nickel-zinc alloys with nanowires morphology cathode for alkaline electrolyzers. Electrodes are obtained by the simple method of template electrosynthesis that is also inexpensive and easily scalable. Through the analysis of the morphological and chemical composition of nanowires, it was found that the nanowires composition is dependent on the concentration of two metals in the deposition solution. Electrocatalytic tests were performed in 30% w/w potassium hydroxide aqueous solution at room temperature. In order to study the electrodes stability, mid-term galvanostatic test was also carried out. All electrochemical tests show that nanowires with about 44.39% of zinc have the best performances. Particularly, at -50 $mAcm^{-2}$, these electrodes have an overpotential 50 mV lower than pure Ni nanowire. NiZn nanowires show also a good stability over time without noticeable signs of performance decay.

KEYWORDS: Alkaline Electrolyzer, Nanowires, Nickel-Zinc Alloy, Hydrogen Evolution Reaction, Template Electrosynthesis, Nanostructured Electrodes.

1 INTRODUCTION

Rethinking the current systems for energy production and distribution on a global scale is one of the main challenges our society has to face in the immediate future. The use of fossil fuels as a primary energy source is leading to a point of no return in terms of greenhouse gas emissions, average global temperature and related phenomena [1,2]. Increasing energy production from renewable sources is a possible solution to these problems [3], however, renewable sources have a weak point due to their randomness. Thus, their coupling with storage systems is indispensable [4–6]. Green hydrogen (hydrogen obtained by water electrolysis using only electricity from renewable sources) is recognized as one of the best storage systems, in terms of environmental sustainability [7–10]. Nevertheless, the electrochemical water splitting is not yet competitive in economic terms due to the cost of the materials, the average life of the electrolyzers, and their efficiency [11]. The report of the International Energy Agency (IEA) estimates the cost of green hydrogen, coupling renewable sources and electrolyzers, between 3.0 and 7.5 USD (Unites States Dollars) per kg, which is substantially higher than the cost of grey hydrogen (obtained by steam reforming of fossil fuels such as coal or natural gas, without CO_2 capture) that is between 0.9 and 3.2 USD per kg [12]. While the grey hydrogen price, substantially linked to the price of coal and natural gas, is not expected to vary much, many scenarios instead foresee a drastic decrease in the cost of green hydrogen, especially in those geographical areas where renewable energy is cheap [13]. In the scenario envisaged by the Energy Transitions Commission (ECT) [14] by 2050, the low price of green hydrogen will allow to cover 80% of the energy demand of industries and 60% of the aviation sector. To achieve this ambitious goal, the ECT foresees that numerous investments will

be necessary to increase the production of energy from renewable sources to be employed for the production of hydrogen, for transport and storage infrastructures and obviously to increase the efficiency of the electrolysers. To increase the efficiency of the three electrolysis technologies (Alkaline Water Electrolysis (AE), Proton-Exchange Membrane Water Electrolysis, High-Temperature Water Electrolysis) [15] it is still necessary to develop innovative materials but also a further optimization of the existing materials used to fabricate the cells. Different approaches have been proposed to overcome the specific problems of the aforementioned technologies [16–19]. Very interesting are, for example, the studies conducted by Sher et al. [20,21] on high temperature electrolysis which is certainly a very promising technology as the better kinetics of the electrode reactions allows to reduce overvoltage and avoid the use of precious materials. Today electrolysis technologies have a different degree of commercial development. Among them, alkaline electrolysers are those widely used for large-scale applications due to their simplicity and relative low cost compared to the others [22]. Currently, the research is focused on improving the AE issues, such as durability and maintenance, in order to reduce the cost of the hydrogen produced [23,24]. A substantial research topic in such regard is the development of new materials for the system electrode/electrocatalyst, in terms of chemical composition and morphological shape, capable of increasing the performance and durability of AE [25–28]. The eligible materials must have some fundamental characteristics, such as good electrocatalytic properties, high conductivity, high availability, ease of supply, low cost, and good chemical stability. In alkaline environment, transition metals are the most suitable electrocatalyst for hydrogen evolution reaction (HER), [29,30]. Among transition metals, the iron group elements are the most commonly used, especially Ni, which is known for its low cost and high chemical stability in alkaline media even if it presents deactivation problems due to the formation of nickel hydride [31]. In order to improve the performance and avoid the deactivation issues, Ni alloys with different metals have been investigated [31,32]. As reported in [33], the activity of Ni alloys

for the HER is: NiMo > NiZn > NiCo > NiW > NiFe > NiCr. In particular, it was demonstrated that NiCo alloys have better electrocatalytic performance compared to pure Ni and Co electrocatalysts [34–36]. Similar conclusions were obtained in the case of NiFe [37,38] and oxidized NiFe [39] for HER and oxygen evolution reaction (OER), respectively. The good performance of Ni alloys was attributed to the elevated number of *d* electrons that ensure high corrosion resistance and electrochemical activity [40,41]. Very interesting is also the NiZn alloy, that is widely used in automotive and aerospace sector for its good mechanical and corrosion-resistant properties [42–44]. However, NiZn alloys are well known for their high electrocatalytic activity for HER, which is only exceeded by NiMo alloys [45]. Herraiz-Cardona et al. [46] have studied the electrocatalytic performance of NiZn and NiZn/Co alloys measuring a very low overpotential of 0.138 V at 250 mA/cm^2. As known, during electrolyzer operation, a partially preferentially dissolution of Zn occurs, leading to a formation of a high porous structure that make the electrode more active [47–49]. To better exploit this phenomenon, before electrolyzer operation, electrodes can be subjected to an initial etching process using high concentrated hot soda [46,50,51] or HCl solutions [52].

The performance of electrocatalysts significantly improves when they are used in the nanostructured morphology [53], This ensures large surface area, good electronic conductivity with the current collector and satisfying porosity, which are the essential requirements for a good electrocatalyst. For example, Pd, Ru, and Co nanoparticles was deposited on Ni foam, showing an improvement of catalytic activity in comparison with pure foam [16, 24]. Bimetallic nickel-cobalt phosphide were supported on Ni foam obtaining a unique morphology consisted of nanosheets that display high performance for HER, with a long-term durability lasting 24 h without deactivation phenomena [55]. Interesting results were also found in the case of CoNi oxyhydroxide nanosheets obtained by electrodeposition followed by electrochemical oxidation [56]. This bifunctional catalyst was tested in alkaline media showing high water splitting

efficiency and stability. Ni nanoparticles coupled with MoO_2 nanosheets self-supported on nickel foam [57] were also tested showing negligible loss, even after were held at -1000 mA cm^{-2} for 172 h. Zhang et al. [52] analysed composite porous Ni foams with NiZn alloy nanocoating, and demonstrated that after annealing and acidic etching, the electrocatalytic activity of this foam was improved compared to simple Ni foam.

In this work, NiZn alloy electrodes, consisting of regular arrays of nanowires, have been fabricated and characterized. The nanostructures were obtained through the template electrosynthesis method which allows to obtain nanowires (NWs) with a surface area about 70 times higher than geometrical one [58]. This manufacturing method has been used for the production of electrodes for different electrochemical devices, such as sensors [59,60], batteries [61,62], solar cell [63,64] and but also for electrolyzers [32,65,66]. In particular, in our recent works we have shown that electrodes with nanowires morphology have very good electrocatalytic behavior due to the very high electrochemical active surface area [34,67]. We have shown that NiCo nanowires can be used with good performance for both hydrogen and oxygen development reaction while NiFe nanowires have excellent performance only for OER. Since cobalt is an extremely dangerous element, we therefore sought an alternative element to it to be alloyed with Ni to fabricate nanostructured electrodes for the HER. In this way it will be possible to build an alkaline electrolyzer with highly performing electrodes but also environmentally compatible. For this aim, NiZn alloys with different composition were obtained by changing the Zn/Ni ratio of the electrodeposition baths. In addition, NWs of pure Ni and Zn were fabricated to better estimate the improvement of the alloys in comparison to single metals. After morphological and chemical characterizations performed through SEM, XRD, and EDS analyses, such electrodes were tested as cathodes in 30 % w/w KOH solution. Their properties were analysed by means of potentiodynamic and galvanostatic experiments. To the best of our knowledge, this article is the first one dealing with the study in AE of

electrodes performance consisting of regular arrays of NiZn alloy nanowires with different compositions.

2 MATERIALS AND METHODS

2.1 Electrode Fabrication

For the fabrication of the nanostructured electrode through template electrosynthesis, polycarbonate membranes (Whatman) were employed as a template. As detailed in our previous works, one of the template surfaces was previously made conductive by gold-sputtering [34,67]. Subsequently, a thin Ni film was electrodeposited as current collector and mechanical support for nanowires. The current collector was obtained by potentiostatic electrodeposition using a Watt's bath (300 gL^{-1} nickel sulphate hexahydrate, 45 gL^{-1} nickel chloride, 45 gL^{-1} boric acid) at pH 3. The NWs were thus obtained by potential-controlled pulse electrochemical deposition in a solution consisting of 30 gL^{-1} of ammonium chloride, 30 gL^{-1} of sodium acetate, 15 gL^{-1} of boric acid and different concentration of nickel sulphate hexahydrate and zinc sulphate heptahydrate at pH 5. For all samples, the total amount of Ni and Zn sulphate was always maintained at 0.6 M. For the electrodepositions, a standard cell with three electrodes was employed. A Pt mesh and a saturated calomel electrode (SCE) were used as counter and reference electrodes, respectively. After the NWs growth, the template was dissolved in pure dichloromethane at room temperature. This step was repeated 4 times, using fresh solvent, to guarantee the total removal of the polycarbonate.

2.2 Electrode Characterization

To investigate the morphology and the atomic composition of the nanostructured electrode, a FEG-ESEM microscope (FEI QUANTA 200), equipped with Energy Dispersive Spectroscopy (EDS, EDAX) probe, was used. EDS analyses were carried out in different areas in order to investigate the uniform composition of NWs. An X-ray diffractometer

(RIGAKU D-MAX 25600 HK) was employed to perform the XRD analyses. Diffraction patterns were obtained with a sampling width of 0.01° and a scan speed of 4.00 °/min, using Ni-filtered Cu Kα radiation (λ= 1.54 Å). The current and tube voltage were set at 40 mA and 40 kV, respectively. The phases were identified by comparison with literature.

The performances of the obtained electrodes were evaluated through electrochemical and electrocatalytic tests that were performed in KOH 30% w/w aqueous solution. The tests were performed in a three electrodes cell using as counter-electrode a Ni sheet (surface area about 20 cm^2) and Hg/HgO as reference electrode. The electrochemical characterization was performed at room temperature e without agitation. All potential values reported in this work have been referred to the reversible hydrogen electrode (RHE) at pH 14. Electrochemical tests were carried out using a Cell Test System (Solartron, Mod. 1470 E) and the data obtained were analysed through MultiStat Software. Electrodes were characterized by cyclovoltammetry (CV, scan rate of 0.005 Vs^{-1}), quasi-steady-state polarization (QSSP, scan rate 0.1667 mVs^{-1}) and galvanostatic-step polarization (GS). Also, galvanostatic polarization tests were carried out to evaluate the mid-term behaviour of nanostructured electrodes.

Each experiment, involving deposition and characterization, was repeated at least three times.

3 RESULTS AND DISCUSSION

3.1 Fabrication and physico-chemical characterization

NWs electrodeposition was performed by potential-controlled pulse electrochemical deposition. Usually, pulsed polarization is employed to replenish the double layer by inverting the polarity of the current. For such purpose, the potential pulse form must be chosen to change only the value of current density, maintaining the same polarity. Moreover, in the case of nanostructures deposition the inversion of current density polarity is essential to control the accumulation of hydrogen gas inside the template channels, that can lead to the formation of nanotubes that have

a lower mechanical resistance compared to nanowires. These expedients allow to obtain at the same time:

- the control of the deposition rate inside the nanopores of the template, with the consequent formation of nanowires with uniform lengths and uniformly distributed on the entire surface of current collector;

- the control of the shape of nanostructures, with the formation of nanowire morphology;

- the control of the chemical composition of the nanowires which, does not change with the length of the same.

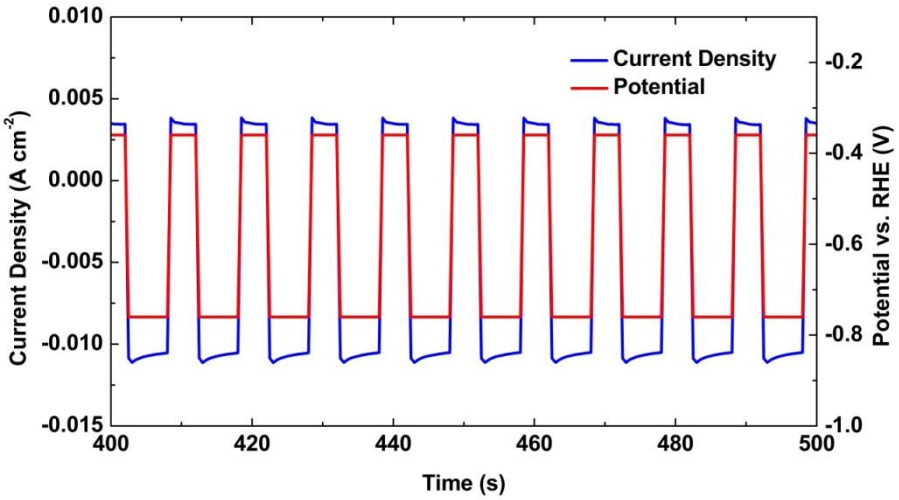

Figure 1. Current density and potential pulse waveform recorded during NWs electrodeposition

After a systematic investigation, we have found that the best conditions correspond to a pulsed polarization between -0.36 and -0.76 V vs. RHE, for 4 and 6 s respectively, up to 50 cycles. The 50 cycles guarantee the formation of NWs of equal length and mechanically stable. For a smaller number of cycles, nanostructures with different lengths are obtained due to the non-uniformity of the initial conditions at the bottom of the template pores [68], while for longer times, too long nanostructures are obtained which in some cases tend to collapse forming bundles on the surface of the electrode.

In Figure 1, the last ten cycles were reported, showing a typical current density response recorded during the electrodeposition of nanowires [69,70]. At -0.76 V vs. RHE, three concomitant reactions occur at electrode/electrolyte interface

$$Ni^{2+} + 2e^- = Ni \quad (1)$$

$$Zn^{2+} + 2e^- = Zn \quad (2)$$

$$2H^+ + 2e^- = H_2 \quad (3)$$

The first two reactions which lead to the formation of NWs of NiZn alloys are desired [71], while the last one is the parasitic HER, which interferes with the reaction of Ni and Zn deposition and originates the formation of nanotubes, due to hydrogen accumulation inside the template channels. Thus, to hinder this parasitic reaction while preserving the advantages above described, after 6 s the potential value was set at -0.36 V vs. RHE. During this period, the template channels are emptied from the gas and the solution inside them is restored.

The composition of nanostructures was tuned by controlling the concentration of Zn and Ni precursors salts in the deposition solution. The total concentration of Ni and Zn was maintained at 0.6 M varying the amount of Ni and Zn in a complementary way, obtaining 7 different electrodeposition baths and thus 7 different types of nanostructured electrodes.

After NWs deposition and template dissolution, NWs composition has been evaluated by EDS analysis. Figure 2 shows the obtained EDS spectra of the different samples. In the spectra, only the peaks relative to Zn and Ni can be observed, indicating the deposition of a pure NiZn alloy not contaminated by other elements present in the deposition solution. To investigate the uniform composition of NWs, different areas of the samples were examined, and a mean value of the atomic composition was calculated. Figure 3 shows the atomic composition of Zn for each electrode as a function of Zn concentration in the deposition bath. Thereafter, the samples will be named with the percentage of Zn composition in the NWs.

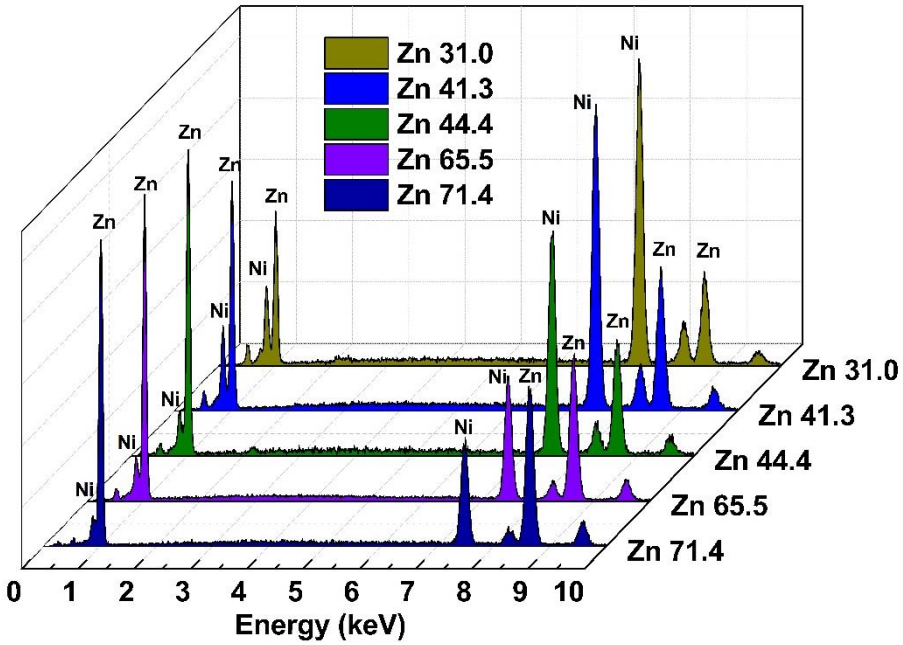

Figure 2. EDS spectra of NWs obtained using electrochemical baths with different composition.

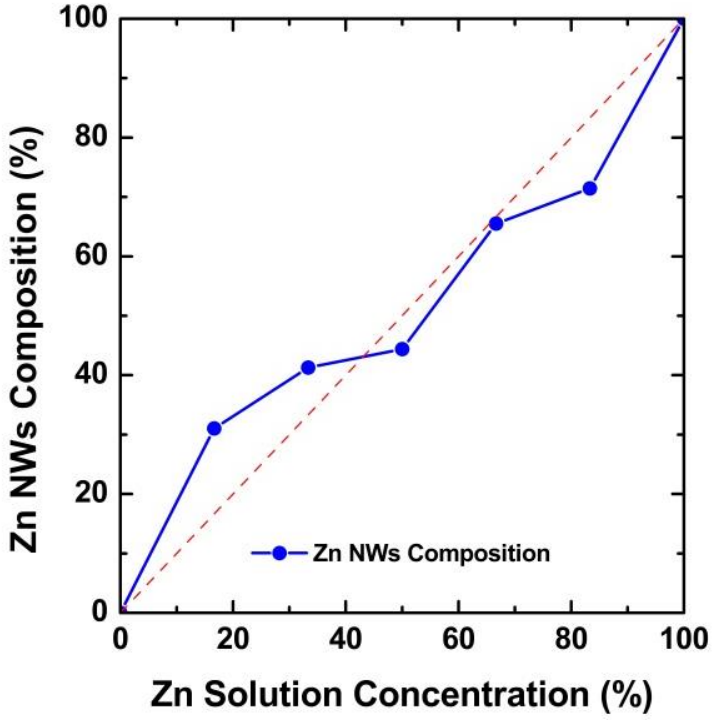

Figure 3. Atomic composition of NWs as a function of Zn concentration in the electrodeposition solutions.

Figure 3 clearly shows that the Zn atomic composition in NWs almost follows the Zn composition in the electrodeposition bath. This behaviour is quite surprising considering that the standard electrochemical redox potentials of the two metals are quite different. In particular, the potential of Ni^{2+}/Ni is 0.04 V vs. RHE, while for Zn^{2+}/Zn is -0.47 V vs. RHE. These thermodynamic values should suggest an easier deposition of Ni in respect to Zn, but this is true only in a simple aqueous solution. For the sample obtained in this work, a deposition bath containing different additives, in particular ammonium chloride and sodium acetate, was used. The presence of both additives explains the Zn content in the NiZn NWs in respect on Zn concentration contained in the deposition bath. In fact, ammonium chloride and sodium acetate are known as good additives that improve the Zn electrodeposition rate.

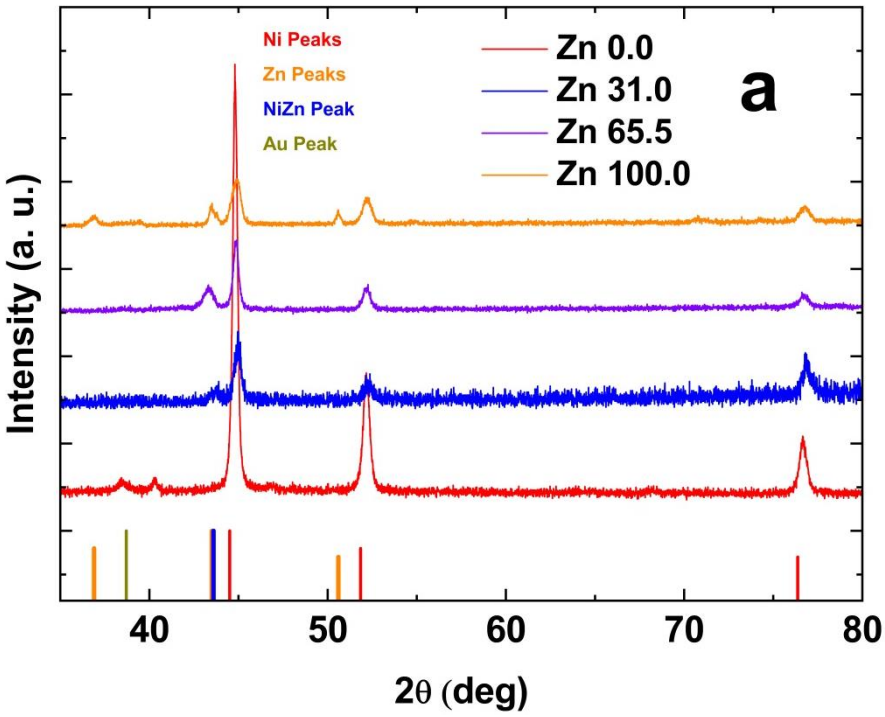

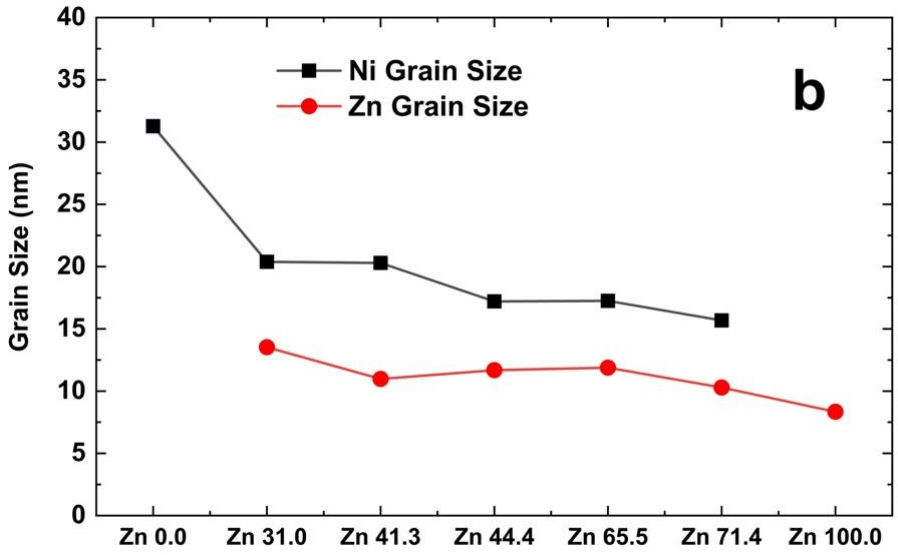

Figure 4. a) XRD patterns of NWs obtained using electrochemical bath with different composition; b) mean NWs grain size calculated by Sherrer's equation.

XRD patterns of some samples are shown in Figure 4a. For pure Ni NWs electrode, the peaks are relative to well crystalline α-Ni with fcc structure. In this pattern, the peak located at about 40° is unknown and it is probably imputable to native oxide of Ni. Ni peaks were detected also for the other electrodes due to the presence of the Ni current collector. For Zn NWs electrode, three peaks have been detected at 36.9°, 43.3°, and 50.6° that are attributable to Zn [72]. For NiZn NWs electrodes, there is a peak in 43.5° [50,73], attributable to NiZn alloy. This peak tends to shift to the right as the Ni concentration increases and its intensity also tends to decrease. As reported in [47] this is due to the incorporation of Zn in the Ni lattice. Using the Sherrer's equation [74], from XRD patterns the mean grain size based on the peak at about 43° and about 45°, respectively imputable to Zn and Ni, was calculated. From pure Ni to alloys a clear decrease (of about 10 nm) of the grain size occurs. As above reported, this is imputable to the presence of Zn in Ni lattice that is also the cause of the broadness of the main Ni peak. Besides, with the increase of Zn concentration the grain size decreases. In the case of Zn grains, the values change very little in the different sample (from about 8 to 13 nm), but they

are always lower compared to Ni. Thus, based these results, it can be concluded that the incorporation of Zn in Ni lattice leads to a formation of NiZn NWs with low crystallinity.

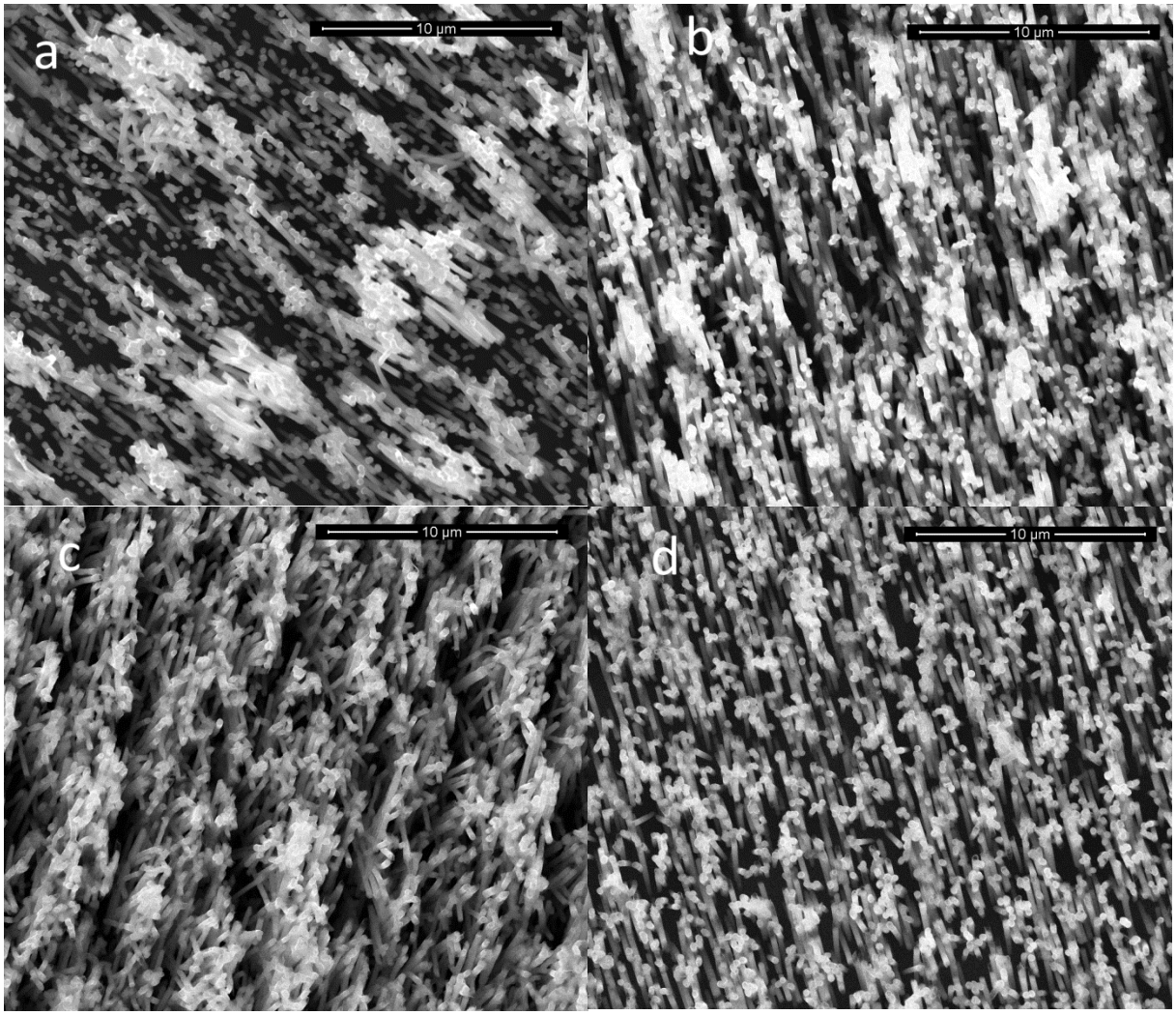

Figure 5. SEM images of NWs obtained using electrochemical bath with different composition: a) Zn 100.0; b) Zn 71.4; c) Zn 65.5; d) Zn 41.3.

In Figure 5, the SEM images of different electrodes were reported. As expected, due to morphology of the template, NWs have a cylindrical shape, with a mean diameter of 220-250 nm and a length of 3-4 µm, and they are highly interconnected. Only pure Zn nanowires (Zn 100.0) differ from this description, and in fact, Figure 5a shows a different morphology. The nanostructures show different length, imputable to the tendency of metallic Zn to dendritic

growth [75], causing different deposition rate, despite the presence of the additives. Figures 5b, 5c and 5d show the morphology for Zn 71.4, Zn 65.5, and Zn 41.3, respectively. NiZn alloy electrodes have greater uniformity than pure Zn NWs. This behaviour is imputable to a stabilization of the deposition rate due to the increase of Ni concentration in the deposition bath [42].

3.2 Electrochemical behaviour

The electrochemical and electrocatalytic behaviour was evaluated by cyclic voltammetry (CV), quasi steady-state polarization (QSSP), galvanostatic-step polarization (GS) and galvanostatic polarization. All tests were performed in 30% w/w KOH aqueous solution at room temperature. The CVs were carried out on scanned range potential from -0.1 to 1.3 V vs. RHE with a scan rate of 5 mVs^{-1} for 5 cycles (Figure 6). As can be observed the first scan is completely different respect to the other except for the electrode consist of pure Ni NWS (Figure 6e Zn 0.0). This behaviour is attributable to the preferential dissolution of Zn [76]. After the CV curves are almost identical to those obtained in the other performed cycles. The obtained results suggest that much of the modification of the electrode occurs immediately after its polarization. This is a good result because it implies that during the operation of the electrolyzer the variation in the composition of the NWs should have little influence, since it happens immediately, Besides, it suggests that it is not necessary an initial dealloying treatment [46,50,51] because it can be done directly in the cell.

Focusing on the fifth cycle of all electrodes, Figure 6f, CV curves show the presence of a couple of redox peaks between 1.2 and 1.3 V and a small anodic peak at 0.1 V. The couple of peaks (1.2 and 1.3 V) is clearly present for all electrodes except in the CV of Zn 100.0. This is an expected result, because as reported in [32,77], these peaks are attributable to the $Ni(OH)_2$/NiOOH couple.

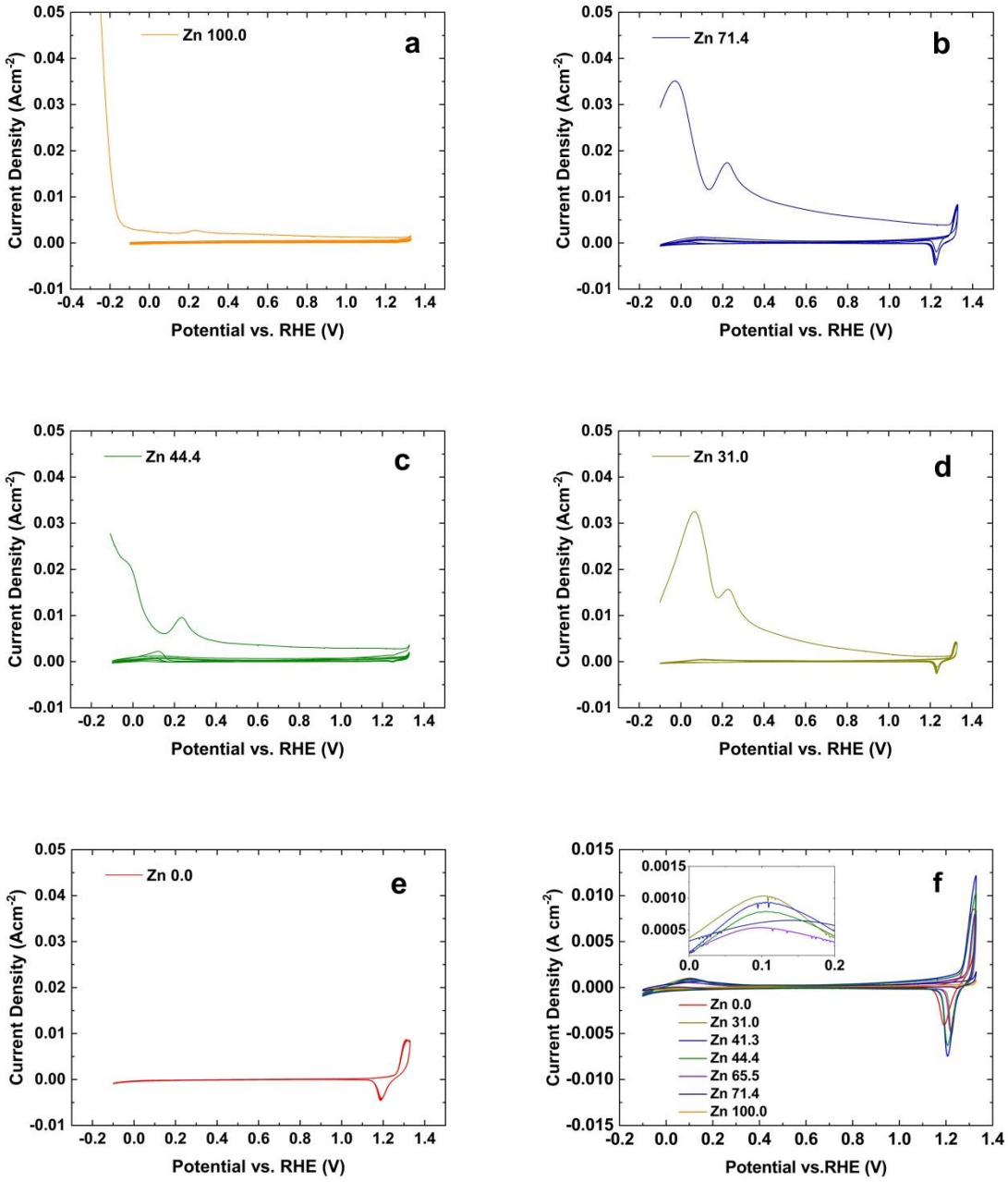

Figure 6. CVs at 5 mVs^{-1} scan rate in 30% w/w KOH aqueous solution at room temperature of NWs obtained using electrochemical baths with different composition: a) Zn 100.0; b) Zn 71.4; c) Zn 44.4; d) Zn 31.0; e) Zn 0.0; f) comparison of the fifth cycle of all electrodes.

The anodic peak at 0.1 V is not present for both Zn 0.0 and Zn 100.0. This peak is related to the oxidation of Zn to $Zn(OH)_4^{2-}$ and it justifies its absence in sample of pure Ni-NWs (Zn 0.0), as confirmed in literature [78]. For the Zn 100.0 sample this peak completely disappears just after

the first scan because a complete dissolution of Zn occurs. Besides, the peak at 0.1 V decreases and widens as the concentration of Zn in the nanostructures increases. This behaviour agrees with the results obtained by Balej et al. [47] that have showed that the dissolution rate of Zn increases with the increase of Zn content in the alloy. The dezincification of the alloy is not a problem, but, on the contrary, as reported by several authors [47–49], it improves the performance of the electrodes because it leads to the formation of more porous, and therefore more active, electrodes.

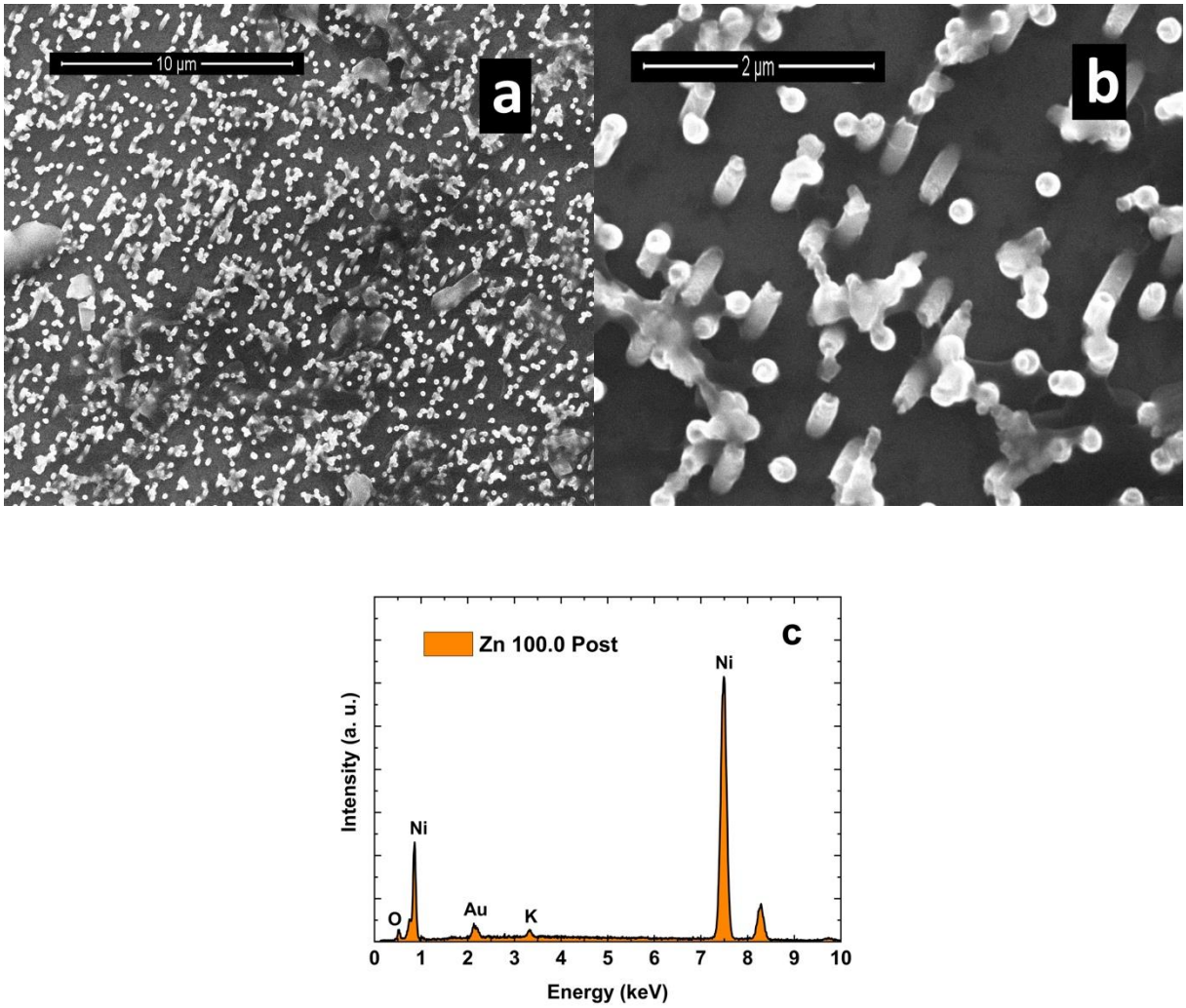

Figure 7. a-b) SEM images and c) EDS spectrum of Zn 100.0 sample after CVs in 30% w/w KOH aqueous solution at room temperature.

SEM images, Figures 7a-b, of the sample Zn 100.0 after CV confirm the complete dissolution of the NWs with the appearance of the surface of the Ni current collector. On its surface, the imprints of small nanowires, really short, can be observed. These are Ni NWs formed during the initial stage of the deposition of the current collector. This statement is proved by the EDS analysis (Figure 7c) that reveals the presence of only Au and Ni, and K traces coming from the contamination of the sample with KOH solution. In the following, we will continue to call this sample Zn 100.0, referring to a Ni substrate with very small nanowires on its surface.

The QSSPs were performed on scanned range potential from 0.1 to -0.9 V vs. RHE with a scan rate of 0.1667 mVs^{-1}. In Figure 8, the only overpotential linear range vs logarithmic current density (reported in absolute value) was shown.

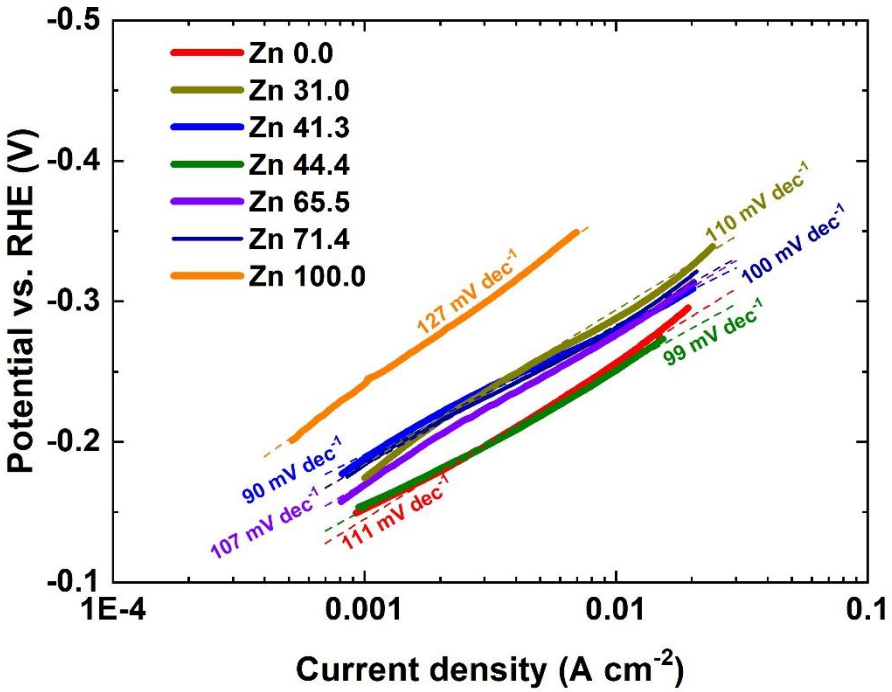

Figure 8. Linear range of QSSPs at -0.1667 mVs^{-1} scan rate in 30% w/w KOH aqueous solution at room temperature of NWs obtained using electrochemical baths with different composition.

By fitting the linear range of QSSP, by means of Tafel's equation (4) [79]

$$\eta = a + b \log i \qquad (4)$$

it is possible to extrapolate the main parameters of η (overpotential activation): a, value related to exchange current density, and b, Tafel's curve slope. These values are listed in Table 1. It is important to highlight that, all b values calculated for our electrodes are much lower than -0.175 $Vdec^{-1}$, listed in Safizadel et al. [31] for a not-nanostructured electrode of the same type of alloy. Besides, our values are lower than -0.168 $Vdec^{-1}$ relative to Ni–Zn (50%) electrodeposited film [22] and lower than a simple Ni sheet, for which a value of -0.142 $Vdec^{-1}$ was calculated [32]. This good behavior of nanostructured electrodes is attributable to the very high number of active sites that characterized the nanostructured morphology [80] that in this case was also improved by the further porosity of the electrode due to the preferential zinc dissolution processes [49]. Our results agree with those of Wang et al. that have shown that good HER catalyst could be obtained also in the case of chemical dealloying of Pt-Co electrodes. For these authors, the dealloying process generates a rough and defective surface Pt-rich which ensures more active Pt sites and thus high HER performance [81].

Table 1. Tafel's parameters of NWs obtained using electrochemical bath with different composition.

Electrode	A	B	Adj. R^2
	V	$Vdec^{-1}$	%
Zn 0.0	-0.478	-0.111	99.54
Zn 31.0	-0.514	-0.110	99.72
Zn 41.3	-0.461	-0.090	99.93
Zn 44.4	-0.449	-0.099	99.66
Zn 65.5	-0.492	-0.107	99.90
Zn 71.4	-0.483	-0.100	99.75
Zn 100.0	-0.621	-0.127	99.92

The electrodes consist of pure Ni (Zn 0.0) and Zn (Zn 100.0) have steeper slopes, while alloyed electrodes have smoother slopes, especially those with an alloy with a slightly richer composition in Ni (Zn 41.3 and Zn 44.4). These findings demonstrate a better electrocatalytic performance of the alloy electrodes compared to NWs of pure elements and are in accordance to the data obtained in the case of thin films of Ni-Zn [76]. The highest value obtained is for the sample Zn 100.0 and this is an expected result given that it is a Ni substrate with small nanowires and therefore with a very small surface area (and consequently the number of active sites). It is however interesting to note that this type of sample, despite the presence of very small NWs, has a smaller Tafel slope than the value calculated for a completely Ni flat plate [32]. The obtained values of Tafel's slope suggest that the hydrogen evolution reaction occurring in these type of electrodes is controlled by the Volmer step [22,82].

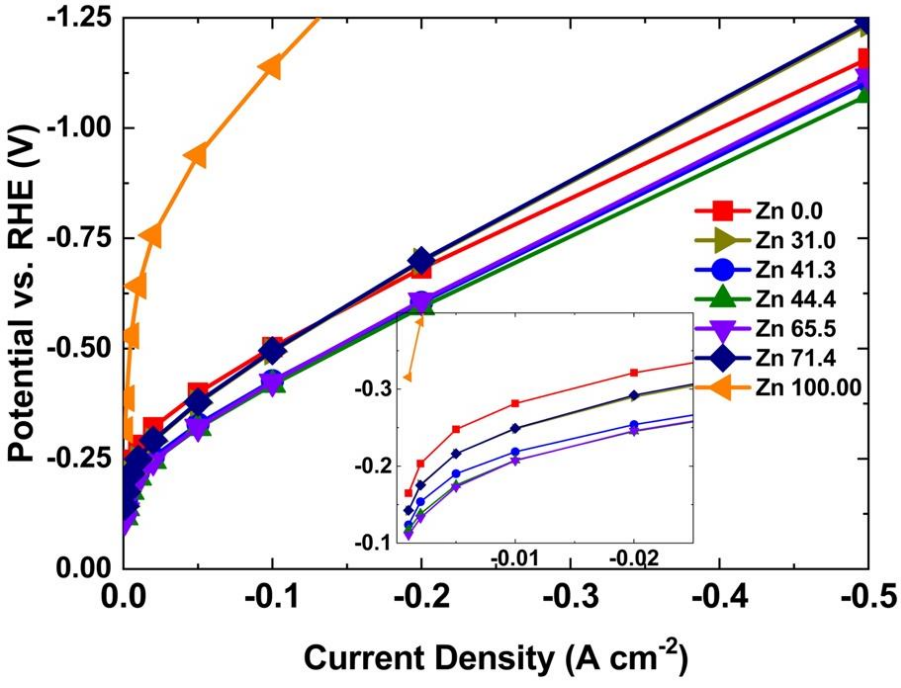

Figure 9. Galvanostatic step test in 30% w/w KOH aqueous solution at room temperature of NWs obtained using electrochemical baths with different composition.

Furthermore, galvanostatic step tests were carried out to evaluate the behaviour of the electrodes at higher current densities. The test consists in the application of increasing current densities performed by a multi current step procedure with a stepwise increase of the current (9 different steps) from a value of -1 to -500 mA cm^{-2} (passing from -2, -5, -10, -20, -50, -100, -200). Each step lasted 5 minutes.

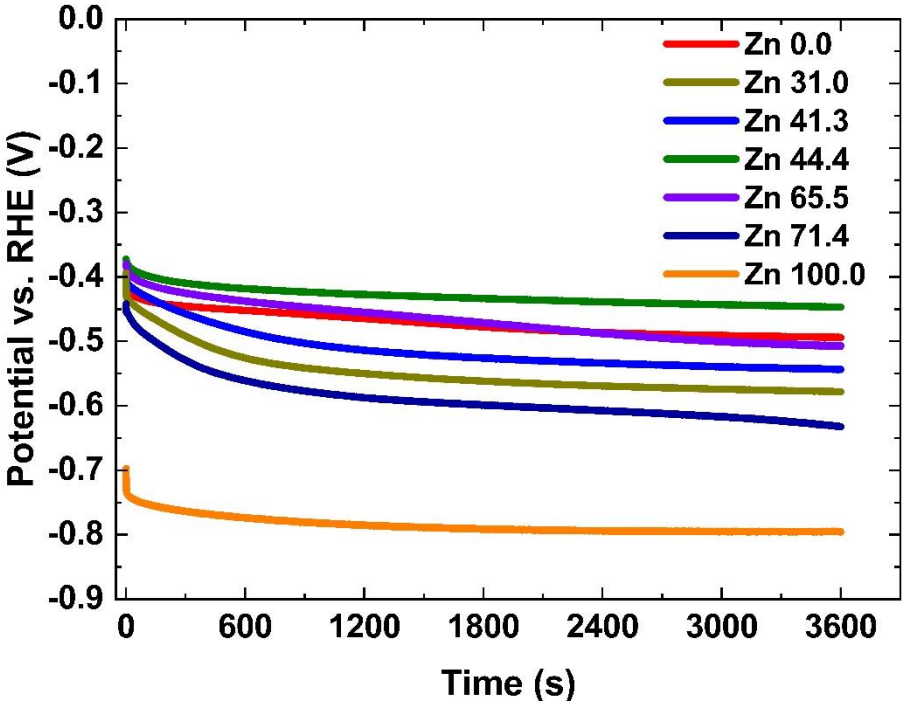

Figure 10. Galvanostatic test conducted at -50 $mAcm^{-2}$ for 1 hour in 30% w/w KOH aqueous solution at room temperature of NWs obtained using electrochemical baths with different composition.

In Figure 9, the values of each step are reported as average value of the measured overpotential. For all investigated current density values, these tests confirm the behaviour of the nanostructured electrodes discussed above. In fact, Zn 100.0 has the worst performance, as expected. In particular, Figure 9 shows a very rapid performance loss which is attributable to the dissolution of Zn nanowires, with the consequent loss of a large part of the electrochemically

active area. As it can be seen from the inset, at low current densities, nanostructured alloy electrodes exhibit similar performances regardless of their composition, thus performing better than pure Ni electrodes. At high current density, alloy electrodes with higher content of Ni and Zn, Zn 31.0 and Zn 71.4, respectively, showed a greater increase in overpotential than the other electrodes. In any case, it can be observed that Zn 44.4 performs slightly better than others throughout the inspected range. These results agree with those obtained by Sheela et al [50], that have also proved that the best alloy composition is that with an initial composition of almost 50% of the two elements.

In order to test the behaviour in a mid-term conditions, galvanostatic tests were carried out for 1 hour at -50 $mAcm^{-2}$. The electrode potential as function of time is shown in Figure 10. The instantaneous decrease of potential can be attributable to preferential dissolution of Zn, that according to CV tests occurs immediately. Also, in this electrocatalytic test, Zn 100.0 shows a much worse performance than the others. As reported in Table 2, Zn 44.4 electrode displays the best performance both in terms of absolute overpotential and potential drop. In fact, a potential drop of about 74.5 mV was measured against 89.9 mV relative to Zn 0.0, while absolute overpotential after 3600 s was approximately 50 mV lower than pure Ni. Thus, these results show that alloying Ni with Zn results in an increased electrocatalytic activity for the HER comparing to pure Ni. This is can be due to the synergism among the catalytic properties of Ni, that is a metal with low hydrogen overpotential, and of Zn, that ensures low hydrogen adsorption free energy [83].

Taking into consideration that the cell potential value of alkaline electrolysers is between 1.8 and 2.4 V [10], a decrease in terms of overpotential of 50 mV would lead to an improvement in energy efficiency of about 1.5-2.2%.

Table 2. Galvanostatic test overpotential values for each electrode and NWs composition after electrochemical tests.

Electrode name	Potential vs. RHE after 1h	ΔV after 1h	Zn Electrode Composition after all tests	Zn loss %
	V	mV	%	
Zn 0.0	-0.493	-89.9	0.0	
Zn 31.0	-0.578	-184.4	5.1	83.5
Zn 41.3	-0.543	-150.3	8.3	79.9
Zn 44.4	-0.446	-74.5	13.3	70.0
Zn 65.5	-0.506	-126.8	19.7	69.9
Zn 71.4	-0.631	-180.6	21.4	70.0
Zn 100.0	-1.045	-98.9	/	

To better evaluate the electrode stability under hydrogen evolution, a longer electrochemical galvanostatic test was conducted for the Zn 44.39 electrode. Figure 11 shows the potential vs. RHE at -50 $mAcm^{-2}$ for a test lasting 18 hours.

After the first 3 hours, the electrode achieves a good stability in terms of potential drop over time. In fact, considering the last 15 hours, every hour the drop is about 2 mVh^{-1}. If we consider the last 10 hours, this value decreases further to 1 mVh^{-1}. As reported in [55], this result can be attributed to a good durability and stability of the electrode which is therefore not subject to chemical-physical modifications during operation which could alter its performance.

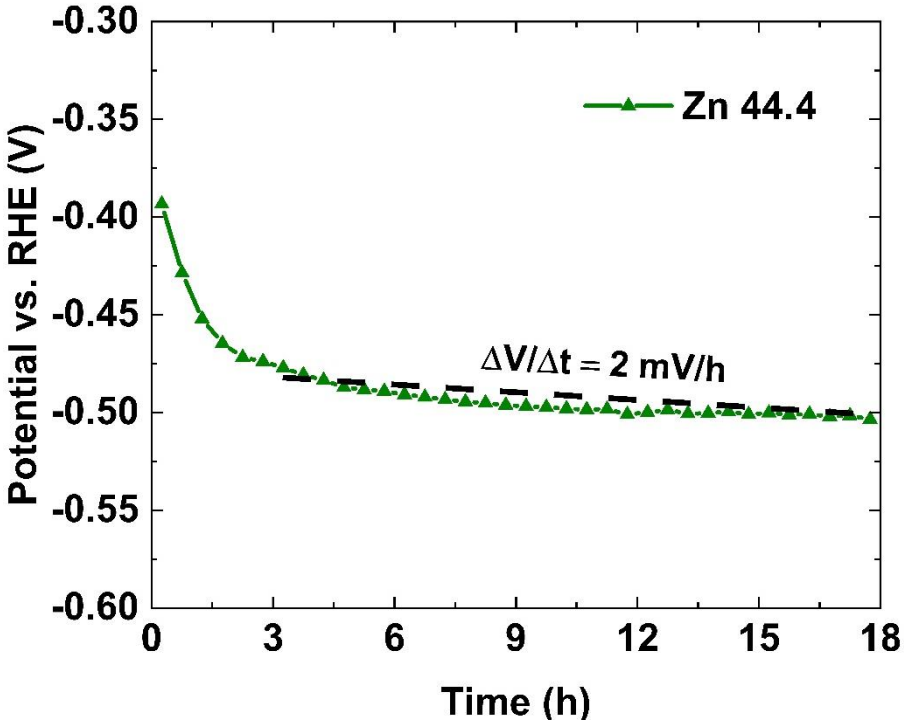

Figure 11. Galvanostatic test of Zn 44.4 sample conducted at -50 $mAcm^{-2}$ for 18 hours in 30% w/w KOH aqueous solution at room temperature.

This very good stability of the alloy electrodes was attributable to the mechanical and chemical stability of the NWs confirmed by the SEM analysis performed after the galvanostatic tests. Although the duration of the test is quite long, the electrodes appear mechanically stable despite the preferential dissolution of Zn that have caused a change in morphology (Figure 12a) and composition (Table 2). As reported in Table 2 and Figure 12b, due to preferential zinc dissolution, NWs become Ni-richer and have a rough surface different from the perfectly smooth one that they have immediately after preparation. As can be observed from the data of Table 2, and according to literature data [47], in the alloys with the high initial Zn content the dissolution of Zn remained almost constant. This behaviour is related to the crystallographic composition of the alloy.

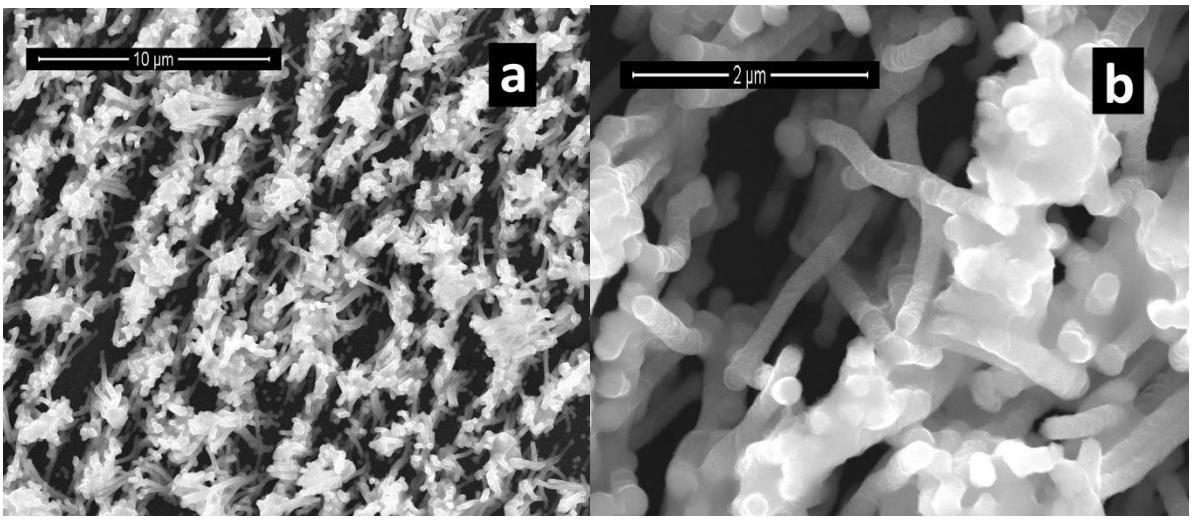

Figure 12. SEM images of NiZn nanowires (Zn 44.4 sample) after operation in 30% w/w KOH aqueous solution at room temperature.

In order to compare the performance of our electrodes with the data present in the literature, in Table 3 the main principal parameters of the electrochemical behaviour of different alloys were reported. For a standard comparison the η_{10} value at a current density of -10 mA cm^{-2} was reported [84]. The performance of our electrodes is almost better than that of many catalysts reported in the Table 3.

Table 3. Comparison of performance of various electrocatalysts (TW: this work)

Electrocatalysts	**KOH solution**	**Tafel slope (mV/dec)**	**Current density (mA/cm^2)**	**η_{10} (V vs. RHE)**	**Ref.**
Ni strip	30 % w/w	-142			[32]
Ni NWs	30 % w/w	-118	-10	-0.250	[32]
$Ni_{0.95}Ce_{0.05}$	8 M	-126	-10	-0.43	[85]
NiS_2 HMSs	1 M	-157	-10	-0.219	[86]
NiCo	30 % w/w	-101	-10	-0.234	[87]
NiZn Foam	30 % w/w	-120	-20	-0.306	[52]
G@Co@Zn@NF-350	1 M	-144	-10	-0.151	[88]
3D Ni Foam	8 M	-105	-10	-0.200	[89]
PTFE Ni-Raney	38 % w/w	-111	-10	-0.208	[90]
FeSe-NF	1 M	-145	-10	-0.200	[91]
p-NiSe/NGr	1 M	-125	-10	-0.285	[92]
$Ni_{0.05}Co_{0.95}$ NWs	30 % w/w	105	-10	-0.231	[34]
$Ni_{78.95}Fe_{21.05}$ NWs	30 % w/w	-116	-10	-0.315	[67]

Ni-Co-P on Ni Foam	1 M	-46	-10	-0.085	[55]
CoNi oxyhydroxide nanosheets	1 M	-67	-10	-0.210	[56]
Ni@C-MoO_2 on Ni Foam	1 M	-44	-10	-0.025	[57]
Ni NWs	**30 % w/w**	**-111**	**-10**	**-0.256**	**TW**
$Ni_{58.7}Zn_{41.3}$ NWs	**30 % w/w**	**-90**	**-10**	**-0.281**	**TW**
$Ni_{55.6}Zn_{44.4}$ NWs	**30 % w/w**	**-99**	**-10**	**-0.251**	**TW**

In comparison with other nanostructured electrodes that we have studied, the NiZn NWs have higher performance than the previously obtained with the NiCo alloy [34], which to date has been the nano-structured alloy with the best performance that we have manufactured for the HER reaction. This result is very important because it would avoid the use of Co that is an extremely toxic metal.

Thus, this type of electrode can be used in an asymmetric electrolyzer that can be assembled with NiZn NWS for HER and NiFe NWs for OER, that is the best nanostructured alloy that we have fabricated for this reaction [67].

4 CONCLUSIONS

In this work, the template electrosynthesis method was employed for the fabrication of nanostructured Ni-Zn alloys. Electrodes were obtained by pulsed electrochemical deposition and consisted of regular arrays of nanowires uniformly distributed on current collector. In order to obtain alloys with different compositions, solutions with different concentrations of Ni and Zn were used. All samples were characterized by SEM, XRD, and EDS analyses before and after electrochemical tests to study their morphology and composition. The formation of alloy was verified by XRD diffraction that reveals a deposit with a low crystallinity. The composition of nanostructures, evaluated by EDS analysis, follows almost linearly the same proportion of Ni and Zn present in the electrodeposition bath.

The nanostructured NiZn alloy electrodes were tested as cathodes for alkaline electrolyzers in 30% w/w KOH aqueous solution at room temperature. The electrocatalytic performance of the different electrodes for HER was evaluated by means of QSSP and galvanostatic step tests. Furthermore, mid-term galvanostatic tests were conducted to estimate the electrodes stability and durability. Due to the partial dissolution of Zn, nanowires of pure Zn immediately dissolve while nanostructured alloys become Ni-richer. All obtained alloys have good electrocatalytic performance compared to electrodes of pure Ni even if the most promising electrodes are those obtained from electrodeposition bath containing an almost similar concentration of Ni and Zn. In particular, the electrodes containing 44.4% of Zn showed the best performance under HER. For this type of alloy, an overpotential ($\eta 10$) of -0.251 mV was measured while the Tafel's slope is -99 mV/dec, suggesting that the HER is controlled by the Volmer step. This electrode shows also good durability and stability because are able to work at a constant current of $-10\ mA/cm^2$ for 18h without deactivation.

The use of NiZn alloys in electrolyzes allows to avoid the consumption of expensive or dangerous materials. Besides, the fabrication process is very simple and easily scalable, making it ideal for large scale applications.

The improvement achieved bodes well for the use of these electrodes in real systems, which would increase their efficiency and consequently their environmental and economic sustainability. It is important to underline that all the tests in this work were carried out at room temperature and without the use of a water flow. These are important parameters that can further improve the obtained results.

In the next future, the research activities will be focused on tests at different temperatures and using cell with both nanostructured electrodes with the aim to simulate the behaviour of a real electrolyzer.

REFERENCES

[1] Rashid M, Mesfer MKA, Naseem H, Danish M. Hydrogen Production by Water Electrolysis: A Review of Alkaline Water Electrolysis, PEM Water Electrolysis and High Temperature Water Electrolysis. Int J Eng Adv Technol 2015;4:80-93.

[2] Hoffert MI, Caldeira K, Benford G, Criswell DR, Green C, Herzog H, et al. Advanced Technology Paths to Global Climate Stability: Energy for a Greenhouse Planet. Science 2002;298:981–7. https://doi.org/10.1126/science.1072357.

[3] Jacobson MZ, Delucchi MA, Bauer ZAF, Goodman SC, Chapman WE, Cameron MA, et al. 100% Clean and Renewable Wind, Water, and Sunlight All-Sector Energy Roadmaps for 139 Countries of the World. Joule 2017;1:108–21. https://doi.org/10.1016/j.joule.2017.07.005.

[4] Chu S, Majumdar A. Opportunities and challenges for a sustainable energy future. Nature 2012;488:294–303. https://doi.org/10.1038/nature11475.

[5] Bussar C, Stöcker P, Cai Z, Moraes Jr. L, Magnor D, Wiernes P, et al. Large-scale integration of renewable energies and impact on storage demand in a European renewable power system of 2050—Sensitivity study. J Energy Storage 2016;6:1–10. https://doi.org/10.1016/j.est.2016.02.004.

[6] Rozzi E, Minuto FD, Lanzini A, Leone P. Green Synthetic Fuels: Renewable Routes for the Conversion of Non-Fossil Feedstocks into Gaseous Fuels and Their End Uses. Energies 2020;13:420. https://doi.org/10.3390/en13020420.

[7] Midilli A, Dincer I. Hydrogen as a renewable and sustainable solution in reducing global fossil fuel consumption. Int J Hydrog Energy 2008;33:4209–22. https://doi.org/10.1016/j.ijhydene.2008.05.024.

[8] Monnerie N, von Storch H, Houaijia A, Roeb M, Sattler C. Hydrogen production by coupling pressurized high temperature electrolyser with solar tower technology. Int J Hydrog

Energy 2017;42:13498–509. https://doi.org/10.1016/j.ijhydene.2016.11.034.

[9] Bocci E, Zuccari F, Dell'Era A. Renewable and hydrogen energy integrated house. Int J Hydrog Energy 2011;36:7963–8. https://doi.org/10.1016/j.ijhydene.2011.01.098.

[10] Carroquino J, Roda V, Mustata R, Yago J, Valiño L, Lozano A, et al. Combined production of electricity and hydrogen from solar energy and its use in the wine sector. Renew Energy 2018;122:251–63. https://doi.org/10.1016/j.renene.2018.01.106.

[11] Schmidt O, Gambhir A, Staffell I, Hawkes A, Nelson J, Few S. Future cost and performance of water electrolysis: An expert elicitation study. Int J Hydrog Energy 2017;42:30470–92. https://doi.org/10.1016/j.ijhydene.2017.10.045.

[12] The Future of Hydrogen. https://www.iea.org/reports/the-future-of-hydrogen

[13] https://www.rechargenews.com/energy-transition/green-hydrogen-will-be-cost-competitive-with-grey-h2-by-2030-without-a-carbon-price/2-1-1001867

[14] https://www.energy-transitions.org/publications/making-clean-hydrogen-possible

[15] Millet P, Grigoriev S. Water Electrolysis Technologies. Renew. Hydrog. Technol., Elsevier; 2013, p. 19–41. https://doi.org/10.1016/B978-0-444-56352-1.00002-7.

[16] Nechache A, Hody S. Alternative and innovative solid oxide electrolysis cell materials: A short review. Renew Sustain Energy Rev 2021;149:111322. https://doi.org/10.1016/j.rser.2021.111322.

[17] Alia SM. Current research in low temperature proton exchange membrane-based electrolysis and a necessary shift in focus. Curr Opin Chem Eng 2021;33:100703. https://doi.org/10.1016/j.coche.2021.100703.

[18] Li C, Baek J-B. The promise of hydrogen production from alkaline anion exchange membrane electrolyzers. Nano Energy 2021;87:106162. https://doi.org/10.1016/j.nanoen.2021.106162.

[19] Zhang S, Zhang X, Rui Y, Wang R, Li X. Recent advances in non-precious metal

electrocatalysts for pH-universal hydrogen evolution reaction. Green Energy Environ 2021;6:458–78. https://doi.org/10.1016/j.gee.2020.10.013.

[20] Sher F, Al-Shara NK, Iqbal SZ, Jahan Z, Chen GZ. Enhancing hydrogen production from steam electrolysis in molten hydroxides via selection of non-precious metal electrodes. Int J Hydrog Energy 2020;45:28260–71. https://doi.org/10.1016/j.ijhydene.2020.07.183.

[21] Al-Shara NK, Sher F, Iqbal SZ, Curnick O, Chen GZ. Design and optimization of electrochemical cell potential for hydrogen gas production. J Energy Chem 2021;52:421–7. https://doi.org/10.1016/j.jechem.2020.04.026.

[22] Zeng K, Zhang D. Recent progress in alkaline water electrolysis for hydrogen production and applications. Prog Energy Combust Sci 2010;36:307–26. https://doi.org/10.1016/j.pecs.2009.11.002.

[23] Brauns J, Turek T. Alkaline Water Electrolysis Powered by Renewable Energy: A Review. Processes 2020;8:248. https://doi.org/10.3390/pr8020248.

[24] Le Bideau D, Mandin P, Benbouzid M, Kim M, Sellier M, Ganci F, et al. Eulerian Two-Fluid Model of Alkaline Water Electrolysis for Hydrogen Production. Energies 2020;13. https://doi.org/10.3390/en13133394.

[25] Zhou D, Li P, Xu W, Jawaid S, Mohammed-Ibrahim J, Liu W, et al. Recent Advances in Non-Precious Metal-Based Electrodes for Alkaline Water Electrolysis. ChemNanoMat 2020;6:336–55. https://doi.org/10.1002/cnma.202000010.

[26] Le Bideau D, Mandin P, Benbouzid M, Kim M, Sellier M. Review of necessary thermophysical properties and their sensivities with temperature and electrolyte mass fractions for alkaline water electrolysis multiphysics modelling. Int J Hydrog Energy 2019;44:4553–69. https://doi.org/10.1016/j.ijhydene.2018.12.222.

[27] Le Bideau D, Chocron O, Mandin P, Kiener P, Benbouzid M, Sellier M, et al. Evolutionary Design Optimization of an Alkaline Water Electrolysis Cell for Hydrogen

Production. Appl Sci 2020;10:8425. https://doi.org/10.3390/app10238425.

[28] Wang L, Weissbach T, Reissner R, Ansar A, Gago AS, Holdcroft S, et al. High Performance Anion Exchange Membrane Electrolysis Using Plasma-Sprayed, Non-Precious-Metal Electrodes. ACS Appl Energy Mater 2019;2:7903–12. https://doi.org/10.1021/acsaem.9b01392.

[29] Gong M, Wang D-Y, Chen C-C, Hwang B-J, Dai H. A mini review on nickel-based electrocatalysts for alkaline hydrogen evolution reaction. Nano Res 2016;9:28–46. https://doi.org/10.1007/s12274-015-0965-x.

[30] Battaglia M, Inguanta R, Piazza S, Sunseri C. Fabrication and characterization of nanostructured Ni–IrO2 electrodes for water electrolysis. Int J Hydrog Energy 2014;39:16797–805. https://doi.org/10.1016/j.ijhydene.2014.08.065.

[31] Safizadeh F, Ghali E, Houlachi G. Electrocatalysis developments for hydrogen evolution reaction in alkaline solutions – A Review. Int J Hydrog Energy 2015;40:256–74. https://doi.org/10.1016/j.ijhydene.2014.10.109.

[32] Ganci F, Baguet T, Aiello G, Cusumano V, Mandin P, Sunseri C, et al. Nanostructured Ni Based Anode and Cathode for Alkaline Water Electrolyzers. Energies 2019;12:3669. https://doi.org/10.3390/en12193669.

[33] Li X, Hao X, Abudula A, Guan G. Nanostructured catalysts for electrochemical water splitting: current state and prospects. J Mater Chem A 2016;4:11973–2000. https://doi.org/10.1039/C6TA02334G.

[34] Ganci F, Cusumano V, Livreri P, Aiello G, Sunseri C, Inguanta R. Nanostructured Ni–Co alloy electrodes for both hydrogen and oxygen evolution reaction in alkaline electrolyzer. Int J Hydrog Energy 2021;46:10082-92. https://doi.org/10.1016/j.ijhydene.2020.09.048.

[35] Colli AN, Girault HH, Battistel A. Non-Precious Electrodes for Practical Alkaline Water Electrolysis. Materials 2019;12:1336. https://doi.org/10.3390/ma12081336.

[36] Hong SH, Ahn SH, Choi I, Pyo SG, Kim H-J, Jang JH, et al. Fabrication and evaluation of nickel cobalt alloy electrocatalysts for alkaline water splitting. Appl Surf Sci 2014;307:146–52. https://doi.org/10.1016/j.apsusc.2014.03.197.

[37] Solmaz R, Kardaş G. Electrochemical deposition and characterization of NiFe coatings as electrocatalytic materials for alkaline water electrolysis. Electrochimica Acta 2009;54:3726–34. https://doi.org/10.1016/j.electacta.2009.01.064.

[38] Flis-Kabulska I, Flis J. Electroactivity of Ni–Fe cathodes in alkaline water electrolysis and effect of corrosion. Corros Sci 2016;112:255–63. https://doi.org/10.1016/j.corsci.2016.07.017.

[39] Bates MK, Jia Q, Doan H, Liang W, Mukerjee S. Charge-Transfer Effects in Ni–Fe and Ni–Fe–Co Mixed-Metal Oxides for the Alkaline Oxygen Evolution Reaction. ACS Catal 2016;6:155–61. https://doi.org/10.1021/acscatal.5b01481.

[40] Santos DMF, Sequeira CAC, Figueiredo JL. Hydrogen production by alkaline water electrolysis. Quím Nova 2013;36:1176–93. https://doi.org/10.1590/S0100-40422013000800017.

[41] Safizadeh F, Ghali E, Houlachi G. Electrocatalysis developments for hydrogen evolution reaction in alkaline solutions – A Review. Int J Hydrog Energy 2015;40:256–74. https://doi.org/10.1016/j.ijhydene.2014.10.109.

[42] Maniam KK, Paul S. Progress in Electrodeposition of Zinc and Zinc Nickel Alloys Using Ionic Liquids. Appl Sci 2020;10:5321. https://doi.org/10.3390/app10155321.

[43] Tafreshi M, Allahkaram SR, Farhangi H. Comparative study on structure, corrosion properties and tribological behavior of pure Zn and different Zn-Ni alloy coatings. Mater Chem Phys 2016;183:263–72. https://doi.org/10.1016/j.matchemphys.2016.08.026.

[44] Conde A, Arenas MA, de Damborenea JJ. Electrodeposition of Zn–Ni coatings as Cd replacement for corrosion protection of high strength steel. Corros Sci 2011;53:1489–97.

https://doi.org/10.1016/j.corsci.2011.01.021.

[45] Raj IA. Nickel-based, binary-composite electrocatalysts for the cathodes in the energy-efficient industrial production of hydrogen from alkaline-water electrolytic cells. J Mater Sci 1993;28:4375–82. https://doi.org/10.1007/BF01154945.

[46] Herraiz-Cardona I, Ortega E, Pérez-Herranz V. Impedance study of hydrogen evolution on Ni/Zn and Ni–Co/Zn stainless steel based electrodeposits. Electrochimica Acta 2011;56:1308–15. https://doi.org/10.1016/j.electacta.2010.10.093.

[47] Balej J, Divisek J, Schmitz H, Mergel J. Preparation and properties of Raney nickel electrodes on Ni-Zn base for H2 and O2 evolution from alkaline solutions Part II: Leaching (activation) of the Ni-Zn electrodeposits in concentrated KOH solutions and H2 and O2 overvoltage on activated Ni-Zn Raney electrodes. J Appl Electrochem 1992;22:711–6. https://doi.org/10.1007/BF01027498.

[48] Cathodic behavior of the dealloyed Ni–Zn coating in sodium hydroxide solution. Int J Corros Scale Inhib 2020;9:334-343. https://doi.org/10.17675/2305-6894-2020-9-1-22.

[49] Solmaz R. Gold-supported activated NiZn coatings: hydrogen evolution and corrosion studies: Gold-supported activated NiZn coatings: HER and corrosion studies. Int J Energy Res 2017;41:1452–9. https://doi.org/10.1002/er.3724.

[50] Sheela G. Zinc–nickel alloy electrodeposits for water electrolysis. Int J Hydrog Energy 2002;27:627–33. https://doi.org/10.1016/S0360-3199(01)00170-7.

[51] Chen L, Lasia A. Study of the Kinetics of Hydrogen Evolution Reaction on Nickel-Zinc Alloy Electrodes. J Electrochem Soc 1991;138:3321–8. https://doi.org/10.1149/1.2085409.

[52] Zhang J, Zhou Y, Zhang S, Li S, Hu Q, Wang L, et al. Electrochemical Preparation and Post-treatment of Composite Porous Foam NiZn Alloy Electrodes with High Activity for Hydrogen Evolution. Sci Rep 2018;8:15071. https://doi.org/10.1038/s41598-018-33205-4.

[53] Mistry H, Varela AS, Kühl S, Strasser P, Cuenya BR. Nanostructured electrocatalysts with tunable activity and selectivity. Nat Rev Mater 2016;1:16009. https://doi.org/10.1038/natrevmats.2016.9.

[54] Pierozynski B, Mikolajczyk T, Kowalski IM. Hydrogen evolution at catalytically-modified nickel foam in alkaline solution. J Power Sources 2014;271:231–8. https://doi.org/10.1016/j.jpowsour.2014.07.188.

[55] Yu C, Xu F, Luo L, Abbo HS, Titinchi SJJ, Shen PK, et al. Bimetallic Ni–Co phosphide nanosheets self-supported on nickel foam as high-performance electrocatalyst for hydrogen evolution reaction. Electrochimica Acta 2019;317:191–8. https://doi.org/10.1016/j.electacta.2019.05.150.

[56] Yu C, Lu J, Luo L, Xu F, Shen PK, Tsiakaras P, et al. Bifunctional catalysts for overall water splitting: CoNi oxyhydroxide nanosheets electrodeposited on titanium sheets. Electrochimica Acta 2019;301:449–57. https://doi.org/10.1016/j.electacta.2019.01.149.

[57] Qian G, Yu G, Lu J, Luo L, Wang T, Zhang C, et al. Ultra-thin N-doped-graphene encapsulated Ni nanoparticles coupled with MoO_2 nanosheets for highly efficient water splitting at large current density. J Mater Chem A 2020;8:14545–54. https://doi.org/10.1039/D0TA04388E.

[58] Inguanta R, Piazza S, Sunseri C. Synthesis of self-standing Pd nanowires via galvanic displacement deposition. Electrochem Commun 2009;11:1385–8. https://doi.org/10.1016/j.elecom.2009.05.012.

[59] Bernardo Patella, Rosalinda Inguanta, Salvatore Piazza, Carmelo Sunseri. Nanowire ordered arrays for electrochemical sensing of h2o2. Chem Eng Trans 2016;47:19–24. https://doi.org/10.3303/CET1647004.

[60] Patella B, Russo RR, O'Riordan A, Aiello G, Sunseri C, Inguanta R. Copper nanowire array as highly selective electrochemical sensor of nitrate ions in water. Talanta

2021;221:121643. https://doi.org/10.1016/j.talanta.2020.121643.

[61] Insinga MG, Oliveri RL, Sunseri C, Inguanta R. Template electrodeposition and characterization of nanostructured Pb as a negative electrode for lead-acid battery. J Power Sources 2019;413:107–16. https://doi.org/10.1016/j.jpowsour.2018.12.033.

[62] Inguanta R, Piazza S, Sunseri C, Cino A, Di Dio V, Cascia DL, et al. An electrochemical route towards the fabrication of nanostructured semiconductor solar cells. SPEEDAM 2010, Pisa, Italy: IEEE; 2010, p. 1166–71. https://doi.org/10.1109/SPEEDAM.2010.5542264.

[63] Battaglia M, Piazza S, Sunseri C, Inguanta R. Amorphous silicon nanotubes via galvanic displacement deposition. Electrochem Commun 2013;34:134–7. https://doi.org/10.1016/j.elecom.2013.05.041.

[64] Ferrara G, Inguanta R, Piazza S, Sunseri C. Characterization of Sn–Co Nanowires Grown into Alumina Template. Electrochem Solid-State Lett 2009;12:K17. https://doi.org/10.1149/1.3059545.

[65] Ganci Fabrizio, Cusumano Valentino, Sunseri Carmelo, Inguanta Rosalinda. Fabrication of Nanostructured Ni-co Electrodes for Hydrogen and Oxygen Evolution Reaction in Water-alkaline Electrolyzer. Chem Eng Trans 2019;73:109–14. https://doi.org/10.3303/CET1973019.

[66] Carmelo Sunseri, Cristina Cocchiara, Fabrizio Ganci, Alessandra Moncada, Roberto Luigi Oliveri, Bernardo Patella, et al. Nanostructured electrochemical devices for sensing, energy conversion and storage. Chem Eng Trans 2016;47:43–8. https://doi.org/10.3303/CET1647008.

[67] Buccheri B, Ganci F, Patella B, Aiello G, Mandin P, Inguanta R. Ni-Fe alloy nanostructured electrodes for water splitting in alkaline electrolyser. Electrochimica Acta 2021;388:138588. https://doi.org/10.1016/j.electacta.2021.138588.

[68] Inguanta R, Piazza S, Sunseri C. Influence of the electrical parameters on the fabrication of copper nanowires into anodic alumina templates. Appl Surf Sci 2009;255:8816–23. https://doi.org/10.1016/j.apsusc.2009.06.062.

[69] Ganci F, Lombardo S, Sunseri C, Inguanta R. Nanostructured electrodes for hydrogen production in alkaline electrolyzer. Renew Energy 2018;123:117–24. https://doi.org/10.1016/j.renene.2018.02.033.

[70] Rosalinda Inguanta, Germano Ferrara, Salvatore Piazza, Carmelo Sunseri. Nanostructure fabrication by template deposition into anodic alumina membranes. Chem Eng Trans 2009;17:957–62. https://doi.org/10.3303/CET0917160.

[71] Schlesinger M, Paunovic M, editors. Modern electroplating. 5th ed. Hoboken, NJ: Wiley; 2010.

[72] Ramanauskas R, Gudavičiūtė L, Kosenko A, Girčienė O, Selskis A. Structural and corrosion characterisation of pulse plated Zn and Zn–Ni alloy coatings. Trans IMF 2012;90:237–45. https://doi.org/10.1179/0020296712Z.00000000045.

[73] Petrauskas A, Grincevičienė L, Češūnienė A, Juškėnas R. Studies of phase composition of Zn–Ni alloy obtained in acetate-chloride electrolyte by using XRD and potentiodynamic stripping. Electrochimica Acta 2005;50:1189–96. https://doi.org/10.1016/j.electacta.2004.07.044.

[74] West AR. Solid state chemistry and its applications. Second edition, student edition. Chichester, West Sussex, UK: Wiley; 2014.

[75] Sharifi B, Mojtahedi M, Goodarzi M, Vahdati Khaki J. Effect of alkaline electrolysis conditions on current efficiency and morphology of zinc powder. Hydrometallurgy 2009;99:72–6. https://doi.org/10.1016/j.hydromet.2009.07.003.

[76] Badawy WA, Nady H, Abd El-Hafez GM. Electrodeposited Zn-Ni alloys as promising catalysts for hydrogen production-Preparation, characterization and electro-catalytic activity.

J Alloys Compd 2017;699:1146–56. https://doi.org/10.1016/j.jallcom.2016.12.228.

[77] Schrebler Guzmán RS, Vilche JR, Arvía AJ. Rate Processes Related to the Hydrated Nickel Hydroxide Electrode in Alkaline Solutions. J Electrochem Soc 1978;125:1578–87. https://doi.org/10.1149/1.2131247.

[78] Trudgeon DP, Qiu K, Li X, Mallick T, Taiwo OO, Chakrabarti B, et al. Screening of effective electrolyte additives for zinc-based redox flow battery systems. J Power Sources 2019;412:44–54. https://doi.org/10.1016/j.jpowsour.2018.11.030.

[79] Bard AJ, Faulkner LR. Electrochemical methods: fundamentals and applications. 2nd ed. New York: Wiley; 2001.

[80] Zhang H, Feng Z, Wang L, Li D, Xing P. Bifunctional nanoporous Ni-Zn electrocatalysts with super-aerophobic surface for high-performance hydrazine-assisted hydrogen production. Nanotechnology 2020;31:365701. https://doi.org/10.1088/1361-6528/ab9396.

[81] Wang F, Yu H, Feng T, Zhao D, Piao J, Lei J. Surface Roughed and Pt-Rich Bimetallic Electrocatalysts for Hydrogen Evolution Reaction. Front Chem 2020;8:422. https://doi.org/10.3389/fchem.2020.00422.

[82] Sorour N, Zhang W, Ghali E, Houlachi G. A review of organic additives in zinc electrodeposition process (performance and evaluation). Hydrometallurgy 2017;171:320–32. https://doi.org/10.1016/j.hydromet.2017.06.004.

[83] Yang Y, Zhu C, Zhou Y, Zhang Y, Xie Y, Lv L, et al. Design and synthesis Zn doped CoP/Co2P nanowire arrays for boosting hydrogen generation reaction. J Solid State Chem 2020;285:121231. https://doi.org/10.1016/j.jssc.2020.121231.

[84] Wang S, Lu A, Zhong C-J. Hydrogen production from water electrolysis: role of catalysts. Nano Converg 2021;8:4. https://doi.org/10.1186/s40580-021-00254-x.

[85] Santos DMF, Amaral L, Šljukić B, Macciò D, Saccone A, Sequeira CAC.

Electrocatalytic Activity of Nickel-Cerium Alloys for Hydrogen Evolution in Alkaline Water Electrolysis. J Electrochem Soc 2014;161:F386–90. https://doi.org/10.1149/2.016404jes.

[86] Tian T, Huang L, Ai L, Jiang J. Surface anion-rich NiS_2 hollow microspheres derived from metal–organic frameworks as a robust electrocatalyst for the hydrogen evolution reaction. J Mater Chem A 2017;5:20985–92. https://doi.org/10.1039/C7TA06671F.

[87] Herraiz-Cardona I, Ortega E, Antón JG, Pérez-Herranz V. Assessment of the roughness factor effect and the intrinsic catalytic activity for hydrogen evolution reaction on Ni-based electrodeposits. Int J Hydrog Energy 2011;36:9428–38. https://doi.org/10.1016/j.ijhydene.2011.05.047.

[88] Jiao M, Chen Z, Zhang X, Mou K, Liu L. Multicomponent N doped graphene coating Co@Zn heterostructures electrocatalysts as high efficiency HER electrocatalyst in alkaline electrolyte. Int J Hydrog Energy 2020;45:16326–36. https://doi.org/10.1016/j.ijhydene.2020.04.121.

[89] Siwek KI, Eugénio S, Santos DMF, Silva MT, Montemor MF. 3D nickel foams with controlled morphologies for hydrogen evolution reaction in highly alkaline media. Int J Hydrog Energy 2019;44:1701–9. https://doi.org/10.1016/j.ijhydene.2018.11.070.

[90] Salvi P, Nelli P, Villa M, Kiros Y, Zangari G, Bruni G, et al. Hydrogen evolution reaction in PTFE bonded Raney-Ni electrodes. Int J Hydrog Energy 2011;36:7816–21. https://doi.org/10.1016/j.ijhydene.2011.01.173.

[91] Chanda D, Tufa RA, Birdja YY, Basu S, Liu S. Hydrothermally/electrochemically decorated FeSe on Ni-foam electrode: An efficient bifunctional electrocatalysts for overall water splitting in an alkaline medium. Int J Hydrog Energy 2020;45:27182–92. https://doi.org/10.1016/j.ijhydene.2020.07.055.

[92] Nadeema A, Walko PS, Devi RN, Kurungot S. Alkaline Water Electrolysis by NiZn-Double Hydroxide-Derived Porous Nickel Selenide-Nitrogen-Doped Graphene Composite.

ACS Appl Energy Mater 2018;1:5500-10. https://doi.org/10.1021/acsaem.8b01081.